SYSTEMS, SCIENCE AND SOFTWARE

A DETERMINISTIC APPROACH TO THE PREDICTION OF FREE FIELD GROUND MOTION AND RESPONSE SPECTRA FROM STICK-SLIP EARTHQUAKES

J. Theodore Cherry
Eldon J. Halda
Kenneth G. Hamilton

Systems, Science and Software
P. O. Box 1620
La Jolla, California 92037

Submitted for Publication in

Earthquake Engineering & Structural Dynamics

December 1974

50272-101

REPORT DOCUMENTATION PAGE	1. REPORT NO. NSF-RA-E-74-505	2.	3. Recipient's Accession No. PB293019
4. Title and Subtitle: Deterministic Approach to the Prediction of Free Field Ground Motion and Response Spectra From Stick-Slip Earthquakes			5. Report Date: December 1974 6.
7. Author(s): J.T. Cherry, E.J. Halda, K.G. Hamilton			8. Performing Organization Rept. No.
9. Performing Organization Name and Address: Systems, Science and Software P. O. Box 1620 La Jolla, California 92037			10. Project/Task/Work Unit No. 11. Contract(C) or Grant(G) No. (C) (G)
12. Sponsoring Organization Name and Address: Applied Science and Research Applications (ASRA) National Science Foundation 1800 G Street, N.W. Washington, D.C. 20550			13. Type of Report & Period Covered 14.

15. Supplementary Notes

16. Abstract (Limit: 200 words)

Theoretical and experimental results from computational physics and nonlinear rock mechanics have been merged in order to obtain a deterministic model of a stick-slip earthquake. The model has been exercised to uncover the dependence of peak ground motion and response spectra on fault length, rupture velocity and dynamic stress drop during rupture. A particular method for generating a design spectrum has been tested against results from the model. Utilization of this deterministic technique seems especially appropriate when design information is required at sites located near the epicenter. This earthquake model furnishes the near source ground motion caused by the stick-slip rupture process. The only limitation in the model is the plane strain assumption which implies an infinite fault dimension normal to the plane. Theoretical seismograms from this model would be appropriate for an earthquake having an out-of-plane fault dimension comparable to the distance between the fault and the building site.

17. Document Analysis a. Descriptors

Earthquakes
Seismology
Earthquake resistant structures
Dynamic structural analysis
Elastic analysis
Buildings

b. Identifiers/Open-Ended Terms

Stick-slip earthquakes
Earthquake engineering

c. COSATI Field/Group

18. Availability Statement	19. Security Class (This Report)	21. No. of Pages
NTIS		47
	20. Security Class (This Page)	22. Price A03 - A01

(See ANSI-Z39.18) See Instructions on Reverse

OPTIONAL FORM 272 (4-77)
(Formerly NTIS-35)
Department of Commerce

SUMMARY

Theoretical and experimental results from computational physics and nonlinear rock mechanics have been merged in order to obtain a deterministic model of a stick-slip earthquake. The model has been exercised to uncover the dependence of peak ground motion and response spectra on fault length, rupture velocity and dynamic stress drop during rupture. A particular method for generating a design spectrum has been tested against results from the model. Utilization of this deterministic technique seems especially appropriate when design information is required at sites located near the epicenter.

INTRODUCTION

The prediction of earthquake ground motion is a central problem associated with the aseismic design of civil engineering structures. Prediction techniques utilized to date[1-5] have been based mainly on the analysis of a very limited number of past earthquake records. Ground motion at a particular site is expected to be strongly influenced by epicentral distance, fault type, earthquake magnitude and local site geology. Therefore, it seems reasonable to question whether the data, furnished by existing earthquake records at epicentral distances less than 20 km, is sufficient to justify empirical or statistical extrapolation of the data for prediction purposes.

In order to both extend the data base and provide a systematic analysis of the factors which control earthquake

ground motion, it is important that techniques be developed which are capable of:

1. Simulating the rupture process during faulting in such a manner that laboratory data from appropriate rock tests may be used to specify the parameters in the rupture model.
2. Calculating the theoretical, free-field seismograms caused by the rupture.
3. Evaluating the modification of the free field ground motion produced by the earth's surface and local site geology.

Computer modeling of the response of geologic materials to a propagating stress wave of arbitrary amplitude is now a standard problem solving technique.[6-9] These computer codes are capable of extending the stress wave, eminating from the source, into the small displacement elastic region[10,11] and yet are flexible enough to permit very general material response formulations in the nonlinear region.[12-15] They have been used to predict the effects of explosive sources on the surrounding rock environment[16-18] and obtain the equivalent elastic source as a function of rock type, depth of burial and explosive yield.[13,19]

In order to at least partially satisfy the above three objectives, a stick-slip rupture model has been incorporated into a two-dimensional (plane strain) stress wave code. The difference equations used in the code for conservation of

linear momentum, strain rate and simulation of a slipping interface are identical to those reported by Cherry, et al.[8]

This earthquake model furnishes the near source ground motion caused by the stick-slip rupture process. The only limitation in the model is the plane strain assumption which implies an infinite fault dimension normal to the plane. Theoretical seismograms from this model would be appropriate for an earthquake having an out-of-plane fault dimension comparable to the distance between the fault and the building site.

The model has been exercised in order to uncover the dependence of peak ground motion and response spectra on fault length, rupture velocity and dynamic stress drop during rupture, i.e., on the important fault parameters which control the release of seismic energy during an earthquake. The theoretical seismograms obtained from this study represent free-field ground motion. They are appropriate to an earthquake occurring in an infinite, homogeneous geologic environment.

Separation of earthquake ground motion into free-field and site amplification components appears to be a natural decomposition.[20] Site amplification effects are capable of being included in the analysis by permitting the free-field ground motion to drive a specific site. Modification of the free-field ground motion by an inhomogeneous, nonlinear

geologic environment will not be addressed in this paper. However, it is important to note that this modification is a natural extension of the computational technique, given the material properties which characterize the local site geology.

SIMULATION OF THE EARTHQUAKE SOURCE

The elastic rebound theory, developed by H. F. Reid after the 1906 San Francisco earthquake, implies that the rupture process at the fault surface is responsible for the relative displacement across the fault and hence the seismic waves radiated during the earthquake. Almost sixty years passed before Benioff[21] showed that the fault displacement inferred from the elastic rebound theory was consistent with seismological observations which suggested that the earthquake source function for the radiated seismic energy should be a double couple. Following Benioff's work, it became clear that an understanding of the nature of the earthquake source depended on an adequate simulation of rupture propagation over the fault surface.

Any formulation of the rupture process must provide quantitative answers to the following three questions:

1. Why does rupture occur?
2. What is the stress adjustment during rupture?
3. When does the rupture heal?

As an added constraint, the rupture model must be able to

accept pertinent laboratory test data in order to specify the parameters in the model.

With this constraint in mind, a stick-slip model of rupture has been formulated which answers the above questions as follows:

1. Rupture initiation is plastic work dependent.
2. During rupture the tangential stress at the slipping interface is relaxed to its kinetic friction value. This relaxation allows adjacent points on the interface to move apart (slip).
3. The rupture heals (adjacent points on the interface stick) if the relative velocity between two adjacent points changes sign and if the tangential stress at the interface is sufficient to maintain continuity of tangential velocity.

The fault surface is simulated by decoupling the grid line over which slip is to occur in order to isolate the normal and tangential components of stress at the interface. Contact discontinuity boundary conditions, involving continuity of normal stress and normal velocity components, are applied in order to solve for the normal stress component.[8] If the boundary point is "welded", i.e., not slipping, then the tangential velocity component will also be continuous. This latter condition permits a unique solution for the tangential stress at the welded point.

The basic mechanism for releasing the strain energy in this rupture model is the relaxation of the tangential stress from its "welded" value to its "kinetic friction" value. Figure 1 follows the tangential stress at two points on the fault surface (slipping interface) during a calculation in which the stick-slip model was used to release the strain energy. For this particular calculation the fault length eventually grew to 10 km. The solid curve in the figure corresponds to the point on the fault where the rupture starts (the focus) while the dashed curve is for a point on the fault 2.5 km away from the focus. The initial value of tangential stress (τ_0) on the fault was one kbar. During rupture this stress component is relaxed to its kinetic friction value (τ_K). In this problem τ_K = 0.5 kbar. The tangential stress is maintained at the τ_k value until adjacent points on each side of the fault reverse velocity. When the velocity reversal occurs, the points are tied (the fault sticks) if the tangential stress, required to maintain continuity of tangential velocity, lies between $\pm \tau_k$. After the points are tied the tangential stress finds a static equilibrium value (τ_s).

Notice that for the point 2.5 km away from the beginning of the fault, the tangential stress builds to a maximum of 1.43 kbar due to stress differences parallel to the fault, before the plastic work criterion at this distance is violated. This occurs at 1.12 seconds; rupture begins and the tangential stress is relaxed to 0.5 kbar.

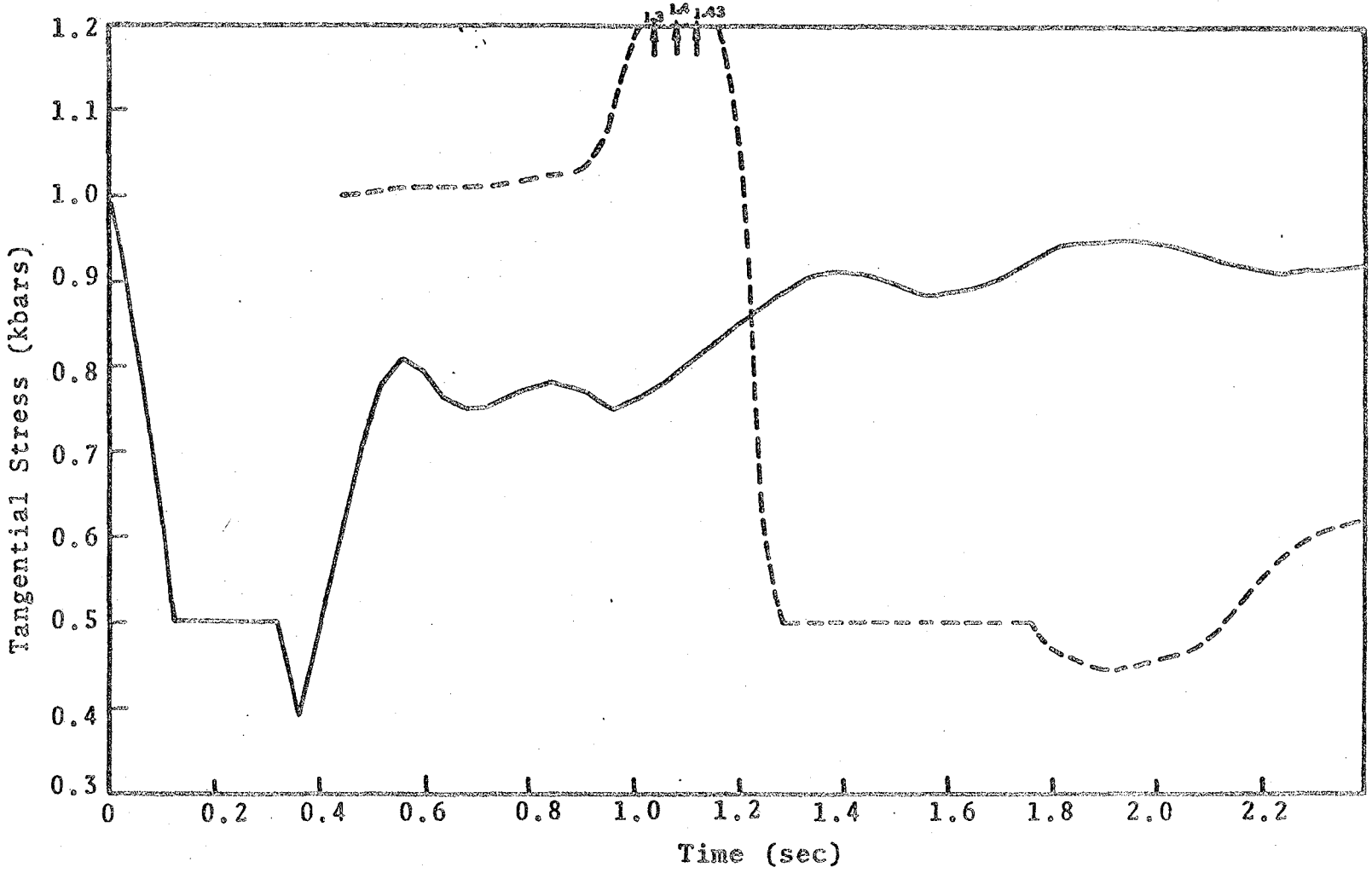

Figure 1. Tangential stress versus time at two points 2.5 km apart from the fault.

Figure 2 shows the final static level attained by the tangential stress over the 10 km fault. Results from all problems run to date indicate that at least one point on the fault will stick early and cause a mild stress concentration to occur in the static solution. In this figure the concentration occurs 3 km from the focus. Figure 2 also shows that most of the static stress drop occurs at the end of the fault where the rupture stops; a result that is again common to all calculations having a finite rupture velocity. The average value of τ_s over the 10 km fault is 0.355 kbar. Therefore, the ratio of static stress drop to dynamic stress drop is 0.29. Due to high frequency attenuation in the earth, teleseismic ground motion and hence teleseismic magnitudes should be sensitive to the long period portion of the source spectrum, i.e., to the static stress drop. The dynamic stress drop on the other hand will be shown to control the peak ground motion in the near field.

Figure 3 shows the relative displacement over the fault at 0.4 second intervals. The point that sticks early, 3 km from the focus, is responsible for the stress concentration at that distance in Fig. 2.

The rupture velocity over the first 7 km of the fault was 2.15 km/sec. At this distance the plastic work criterion was increased so that the rupture would not stop abruptly. Figure 4 shows the arrival time of the rupture versus distance along the fault. Over the last 3 km the rupture velocity is

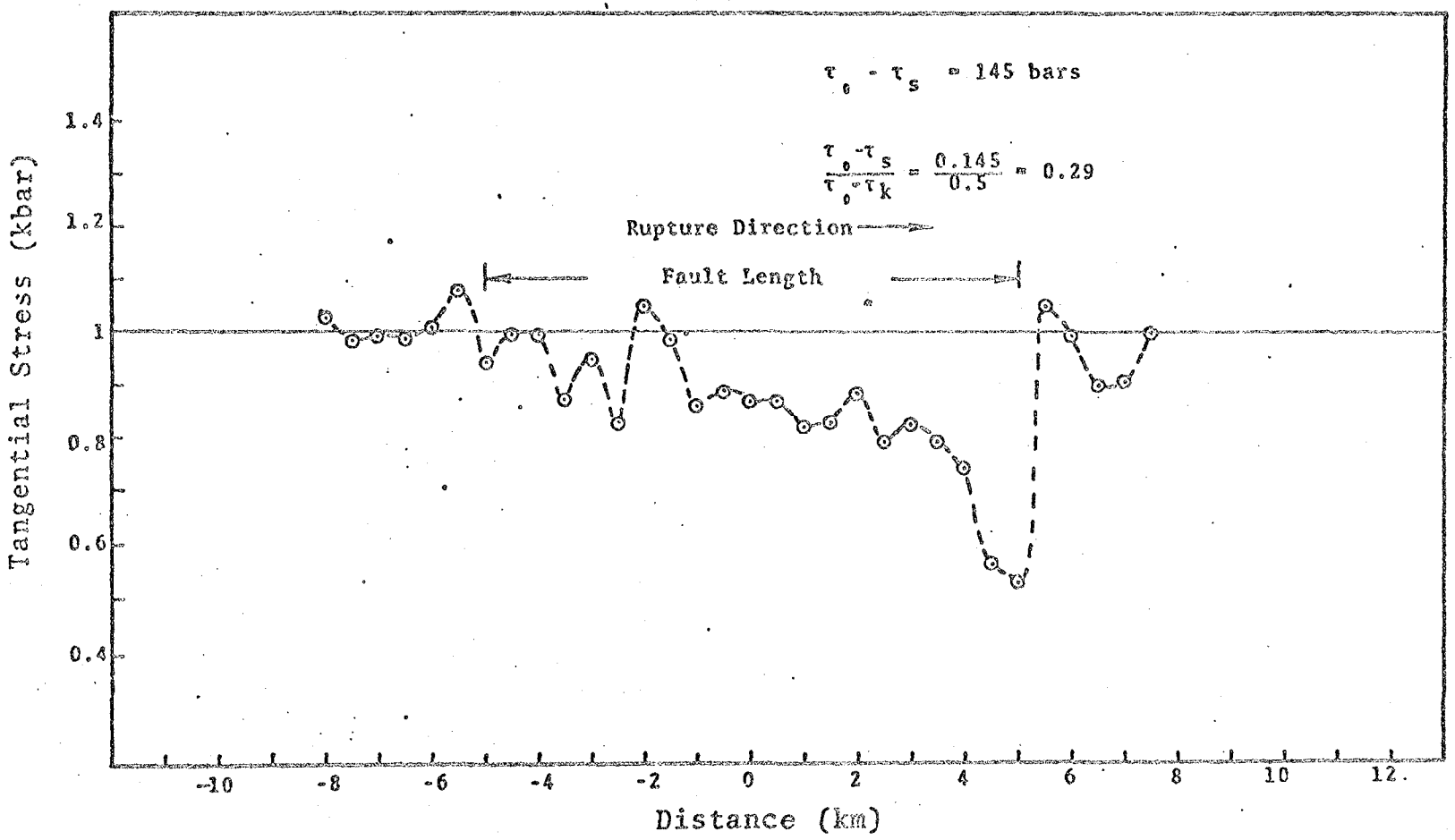

Figure 2. Static value of tangential stress on the fault.

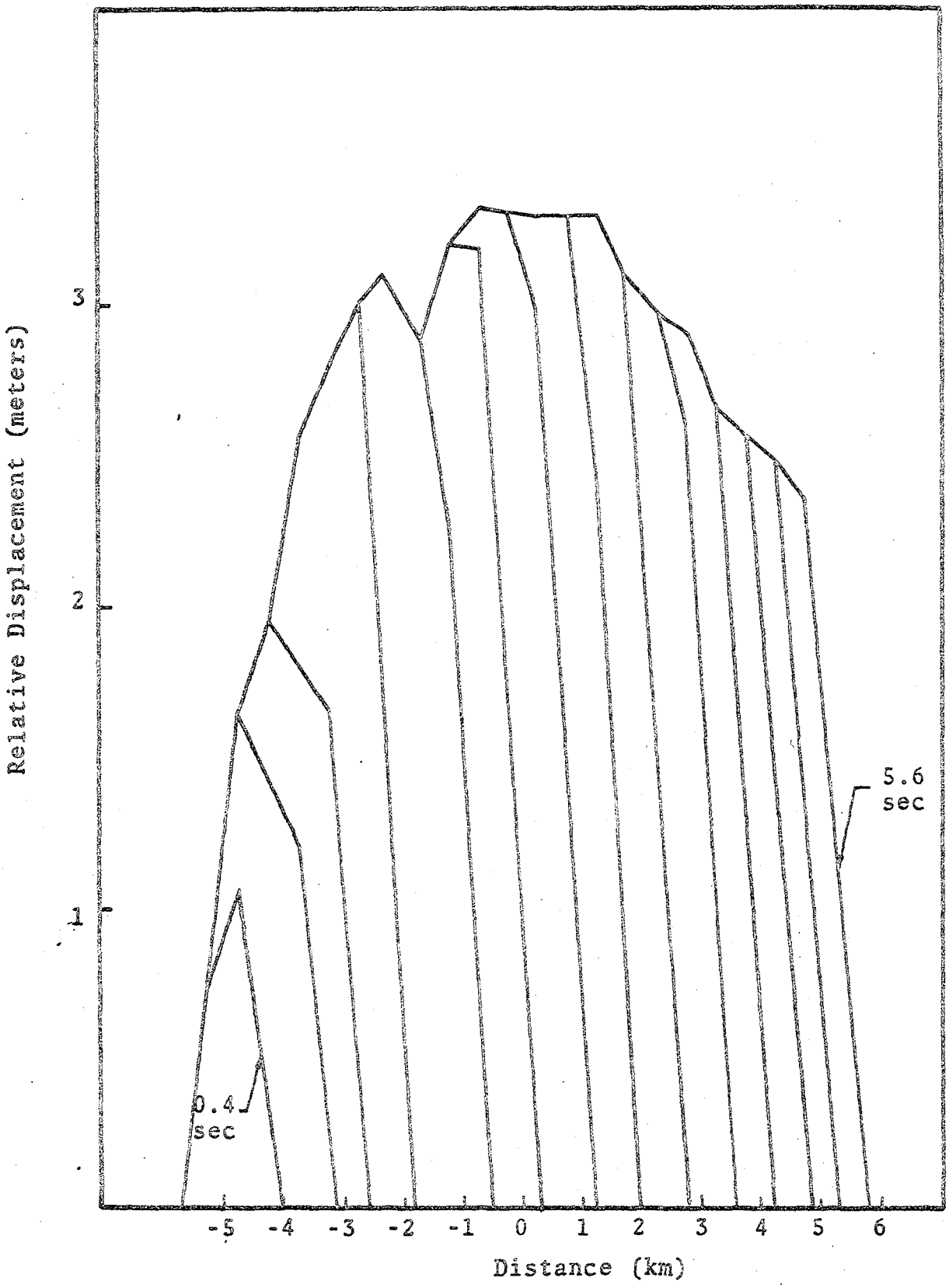

Figure 3. Relative displacement on 10 km fault at 0.4 second intervals.

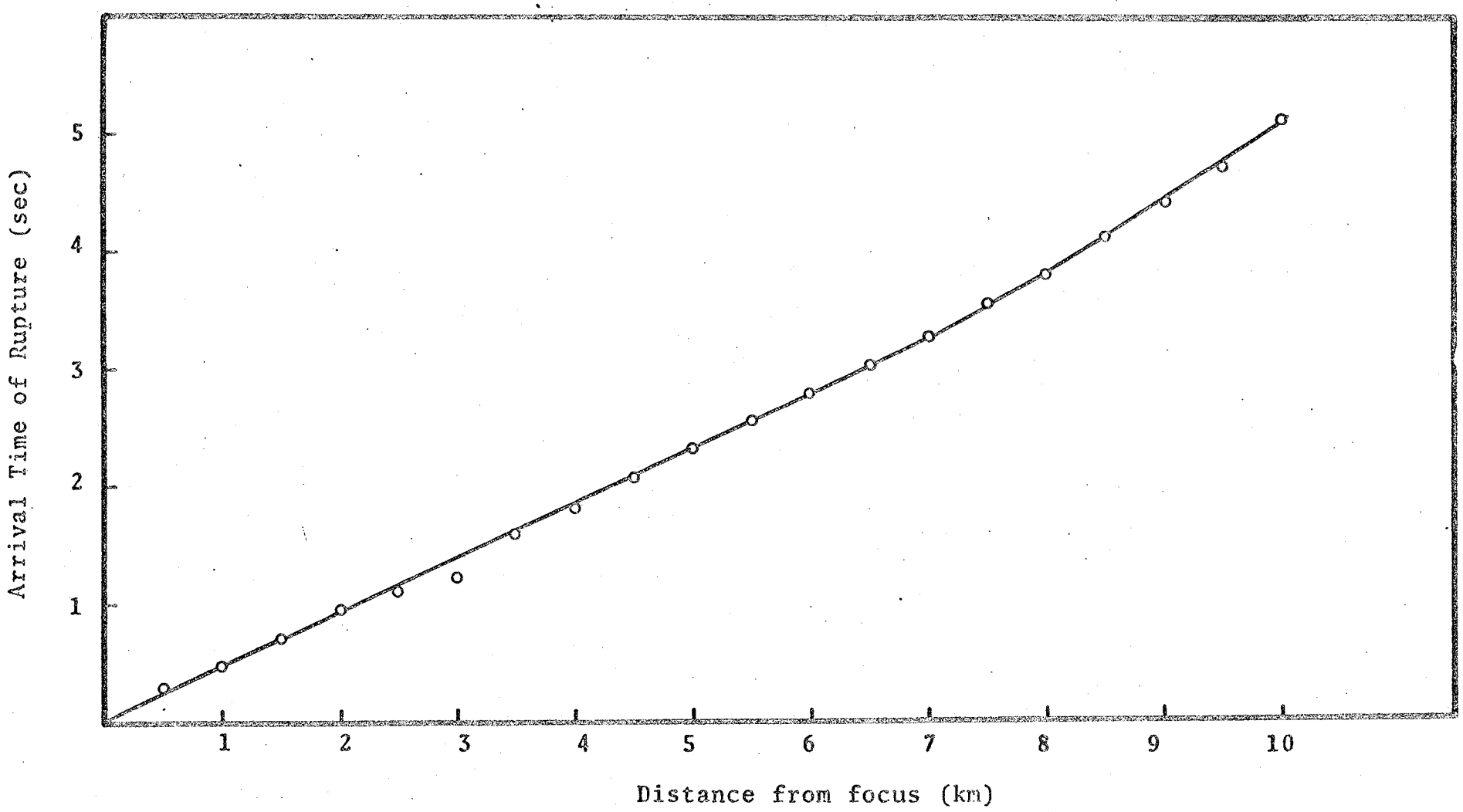

Figure 4. Arrival time of the rupture versus distance along the fault.

approximately 1.6 km/sec, giving an average rupture velocity over the entire fault of 2 km/sec.

Plastic flow is caused by the inability of real geologic materials to support unlimited values of shear stress. The deviatoric stress component in the yielding element are modified such that the resulting stress state is consistent with a Mises yield criterion (Eq. 1, Appendix I).

Initially, plastic flow was included in the model in order to remove the large stress concentrations that occurred at the ends of the rupture during calculations involving only linear, elastic material behavior. It was immediately found that rupture velocity could be controlled by allowing rupture initiation to be dependent on the plastic work dissipated during the yielding process (Eqs. 3 through 5, Appendix I).

Heard[22] has obtained experimental data showing that crystalline rocks undergo significant yielding prior to brittle failure at the temperatures and pressures appropriate even for shallow earthquakes (focal depths of around 10 km). We have allowed this mechanism to control the rupture velocity by specifying the plastic work for rupture to be a function of distance from the focus (Eq. 6, Appendix I). This requires not only that the dimensions of the fault zone be specified, but also the relation between the yield surface and the stress state in the fault zone.

The calculations reported in the next section assumed an elliptical fault zone with all the material in the fault

zone initially lying on the yield surface, i.e., an attempt to increase the second deviatoric stress invariant above its initial value in the fault zone causes plastic flow and therefore plastic work.

The fault model is not restricted to a plastic work rupture criterion. Since the components of stress have been isolated at the fault surface then a rupture criterion could easily be formulated in terms of these stress components.

For example, the tangential stress could initially be limited at the boundary. This would allow the fault to slide stably, i.e., creep. In Fig. 1 creep would occur at a given distance from the focus if the allowable tangential stress were less than 1.0 kbar. The drop in tangential stress to its kinetic friction value (rupture) could then be made a function of the size of the creep event. Stable sliding has been observed, prior to rupture, in laboratory stick-slip events in plates of Westerly granite.[23] Creep may prepare the fault surface for rupture by polishing the surface. Rupture velocity could be controlled by varying the magnitude of the creep event required to cause the tangential stress to drop to its kinetic friction value.

Frictional sliding on ground surfaces of granite has been investigated by Byerlee.[24] For values of normal stress (σ_n) varying between 2 - 12 kbar over the surface, he found that the tangential stress drop from static friction (τ_0) to kinetic friction (τ_k) is given by

$$\tau_0 - \tau_K = 0.25 + 0.13\ \sigma_n \quad \text{(all units in kbars)} \quad (1)$$

While this relation was established for specimens at room temperature and for specially prepared surfaces, it probably furnishes an upper limit to the allowable dynamic stress drop for shallow earthquakes. This stress drop was assumed to be either 0.25 or 0.5 kbar for the calculations discussed in the next section.

SUMMARY OF INPUT PARAMETERS

In order to exercise the rupture model in its current form, a number of parameters must be specified. These are:

- The Fault Zone. An elliptical fault zone, defined as

$$\frac{x^2}{a^2} + \frac{y^2}{b^2} = 1 \quad (2)$$

was assumed with all the material in the fault zone initially lying on the yield surface. The origin of the x-y coordinate system is located at the center of the fault, as shown in Fig. 5. Elastic behavior was assumed for the material outside the fault zone. The minor axis, b, was 2 km for all calculations. The major axis, a, extended 3 km beyond the end of the fault.

- The Plastic Work Required for Rupture Initiation. A unidirectional rupture was assumed as shown in Fig. 5. For a given fault length, L, the functional

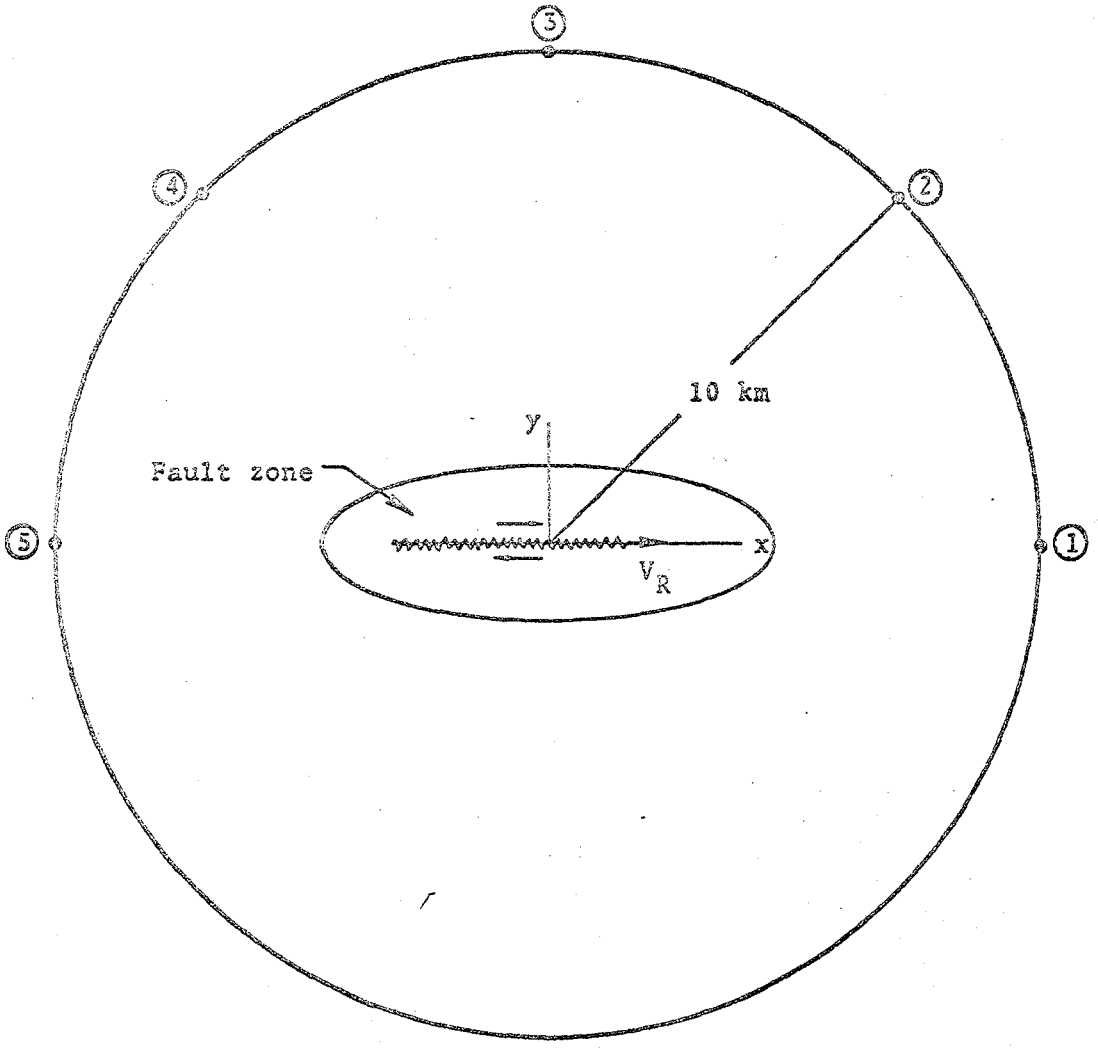

Figure 5. Stations monitored during the calculations. The origin of the x-y coordinate system in the center of the fault. The computational grid extends beyond the 10 km radius in order that reflection from external boundaries do not interfer with the free field ground motion.

form used to initiate rupture within the interval $-L/2 \leq x \leq L/2$ was assumed to be (Appendix I, Eq. 6)

$$W = 6c\left(\frac{x+L/2}{d}\right)\left[\frac{1}{2} - \frac{1}{3}\frac{x+L/2}{d}\right] \qquad \left(0 \leq x + \frac{L}{2} \leq \frac{d}{2}\right) \qquad (3a)$$

$$W = \frac{c}{2}\left[-\frac{1}{2} + 3\frac{x+L/2}{d}\right] \qquad x + \frac{L}{2} \geq \frac{d}{2} \qquad (3b)$$

Rupture starts at $x = -L/2$ ($W = 0$) and is assumed to terminate at $x = L/2$. In the calculations, rupturing was not permitted outside the interval $-L/2 \leq x \leq L/2$.

- The Stress Drop During Rupture ($\tau_0 - \tau_k$). It was found that the normal stress (σ_n) on the fault did not change from its initial value during the calculation. Therefore, the assumed stress drop remained constant over the fault. Equation (1) was used as a guide for this quantity and calucations were obtained for stress drops of 0.25 and 0.5 kbars. The initial stress (τ_0) was the same for all calculations with $\tau_0 = 1$ kbar.
- The Shear Modulus (μ), Bulk Modulus (k) and Density (ρ). These quantities were maintained constant for all calculations, with $\mu = 324$ kbar, $k = 478$ kbar and $\rho = 2.8$ g/cc. The corresponding compression and shear wave velocities are $\alpha = 5.7$ km/sec, $\beta = 3.4$ km/sec.

Table I summarizes the input parameters (a, c, d, L, $\tau_0 - \tau_K$) along with the rupture velocity (V_R) and the average static stress drop ($\tau_0 - \tau_s$) that resulted from the four calculations. Since α, β, ρ, b, and τ_0 were the same for all calculations, these parameters are not listed in the table.

TABLE I

Calculation	a(km)	c	d(km)	L(km)	$\tau_0 - \tau_K$ (kbar)	V_R (km/sec)	$\tau_0 - \tau_s$ (kbar)
10A	8	0.7	10	10	0.5	2.0	0.145
5A	5.5	0.7	10	5	0.5	2.15	0.178
5B	5.5	0.4	10	5	0.5	3.75	0.224
5C	5.5	0.4	10	5	0.25	2.15	0.110

GROUND MOTION AND RESPONSE SPECTRA

All ground motion calculations are easily separable into compressional (P) and shear (S) components. This is accomplished by monitoring the divergence ($\nabla \cdot \vec{s}$) and curl ($\nabla \times \vec{s}$) of the displacement field at selected points in the elastic regime. These components are shown in Figs. 6 and 7 for calculation 5B. These figures give the peak values of the scalar and vector potentials at all stations located 10 km from the center of the fault. The finite rupture velocity produces a noticable distortion in the radiation pattern, with the S component in the fault plane (direction of rupture) approximately twice as large as the S component

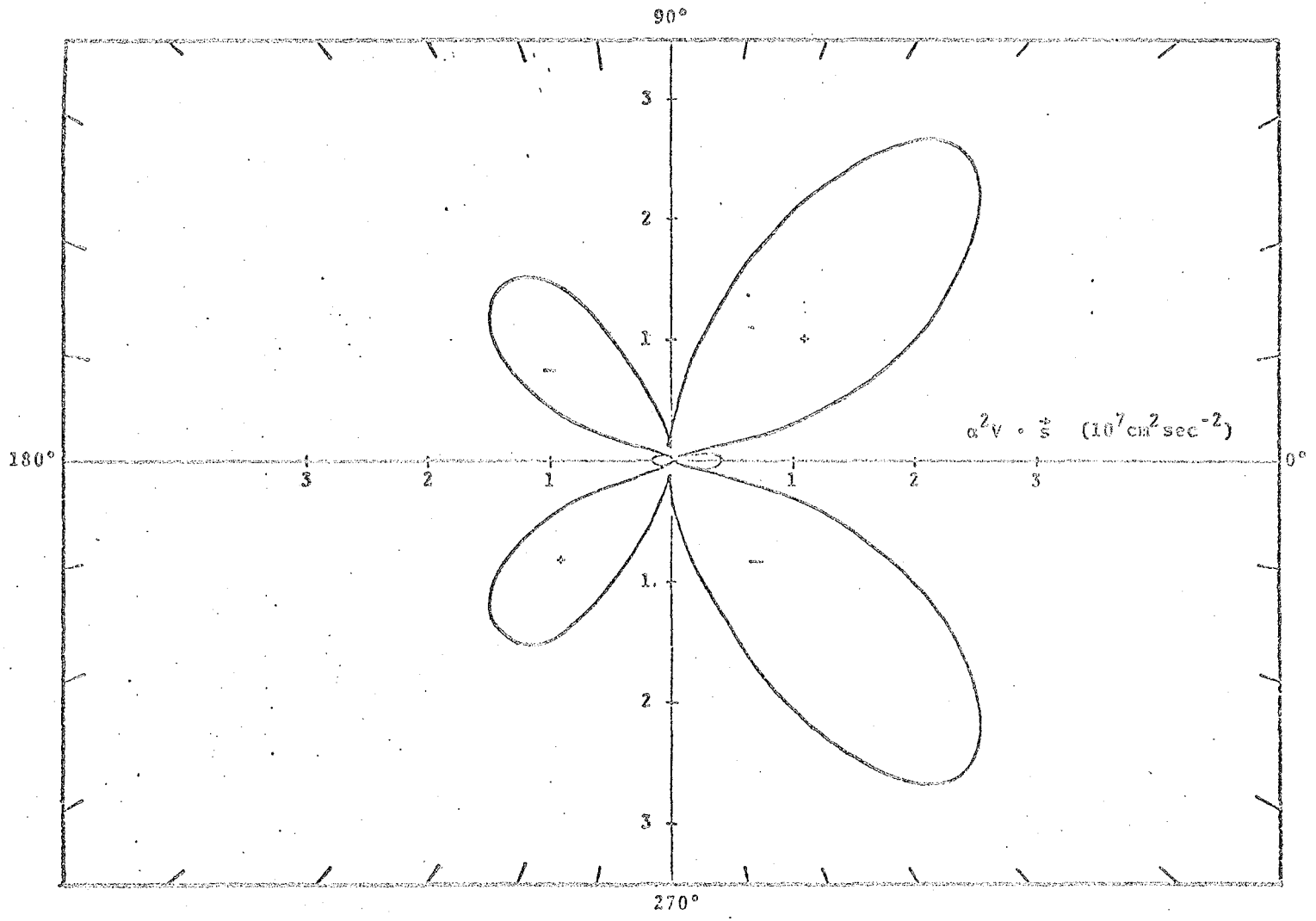

Figure 6. P wave radiation from calculation 5B, compression lobes are denoted by + and rarefaction lobes by −.

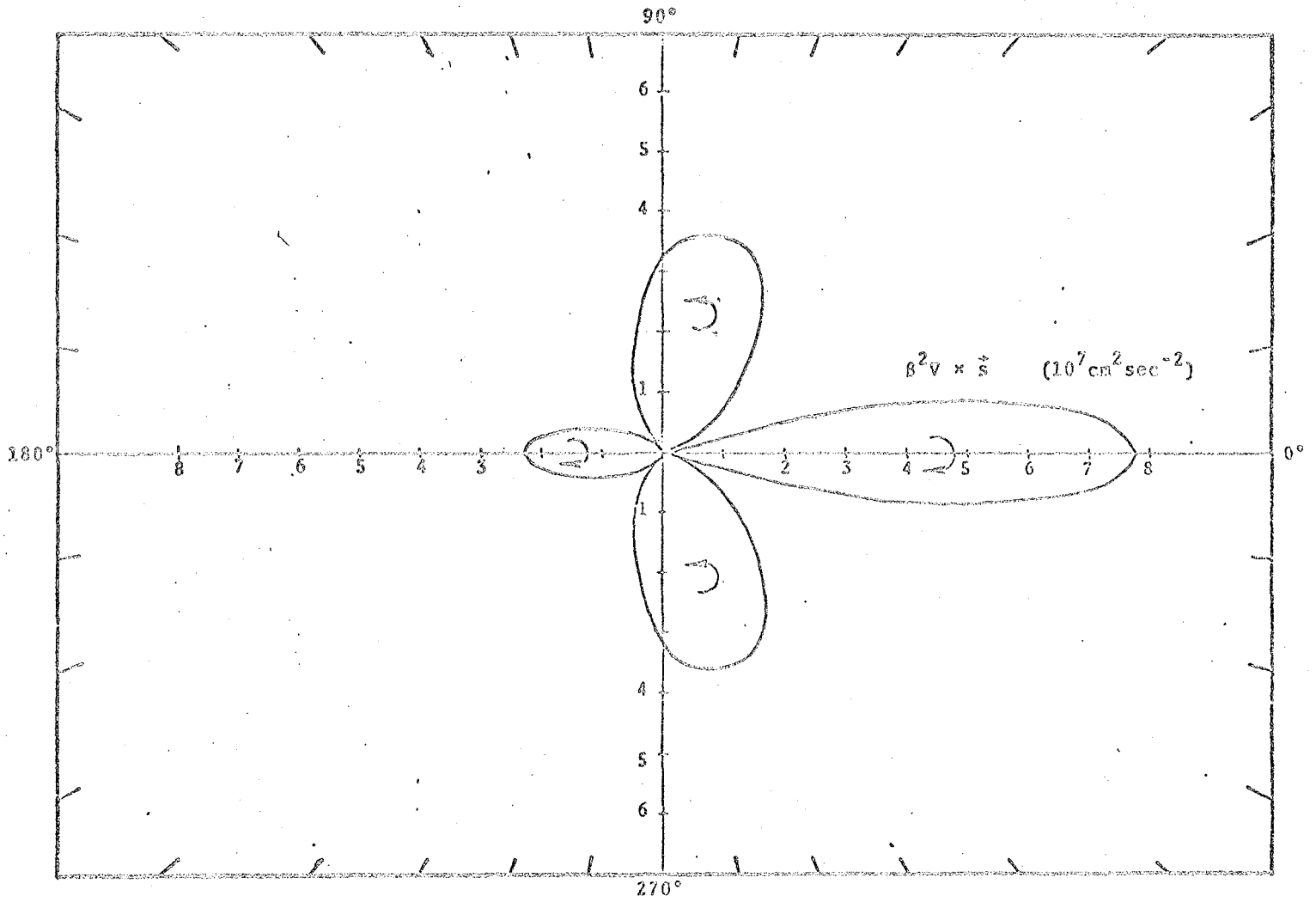

Figure 7. S radiation from calculation 5B. The body rotation is shown for each lobe.

in the auxiliary plane. The same factor applies to the S_{max}/P_{max} ratio.

Figures 8 and 9 show particle velocity time histories at Stations 1 and 5 for calculation 5B. The stations were chosen since they illustrate the maximum azimuthal variation in ground motion between all monitored grid locations. Seismogram complexity increases with increasing station number (1 through 5) due to the temporal separation of the starting and stopping phases of the propagating rupture. This separation results in a factor of seven difference in peak particle velocity between the two stations.

In Fig. 10 the ground motion at Station 1 is compared with the maximum horizontal component of ground motion recorded at Pacoima Dam from the San Fernando earthquake of February 9, 1971. This comparison along with the radiation patterns shown in Figs. 6 and 7 support Hank's[25] conclusion that, "the large displacement pulse occurring at Pacoima Dam approximately 2.5 seconds after the acceleograms were triggered denotes the arrival of shear radiation eminating from massive but localized faulting in the hypocentral region." The simple nature of the seismogram within this time interval also suggests that the rupture propagated toward Pacoima Dam and hence the peak ground motion should be anomalously high at this site.

Figures 11, 12 and 13 give the response spectra at Station 5 from calculation 5B for 1 percent, 5 percent and

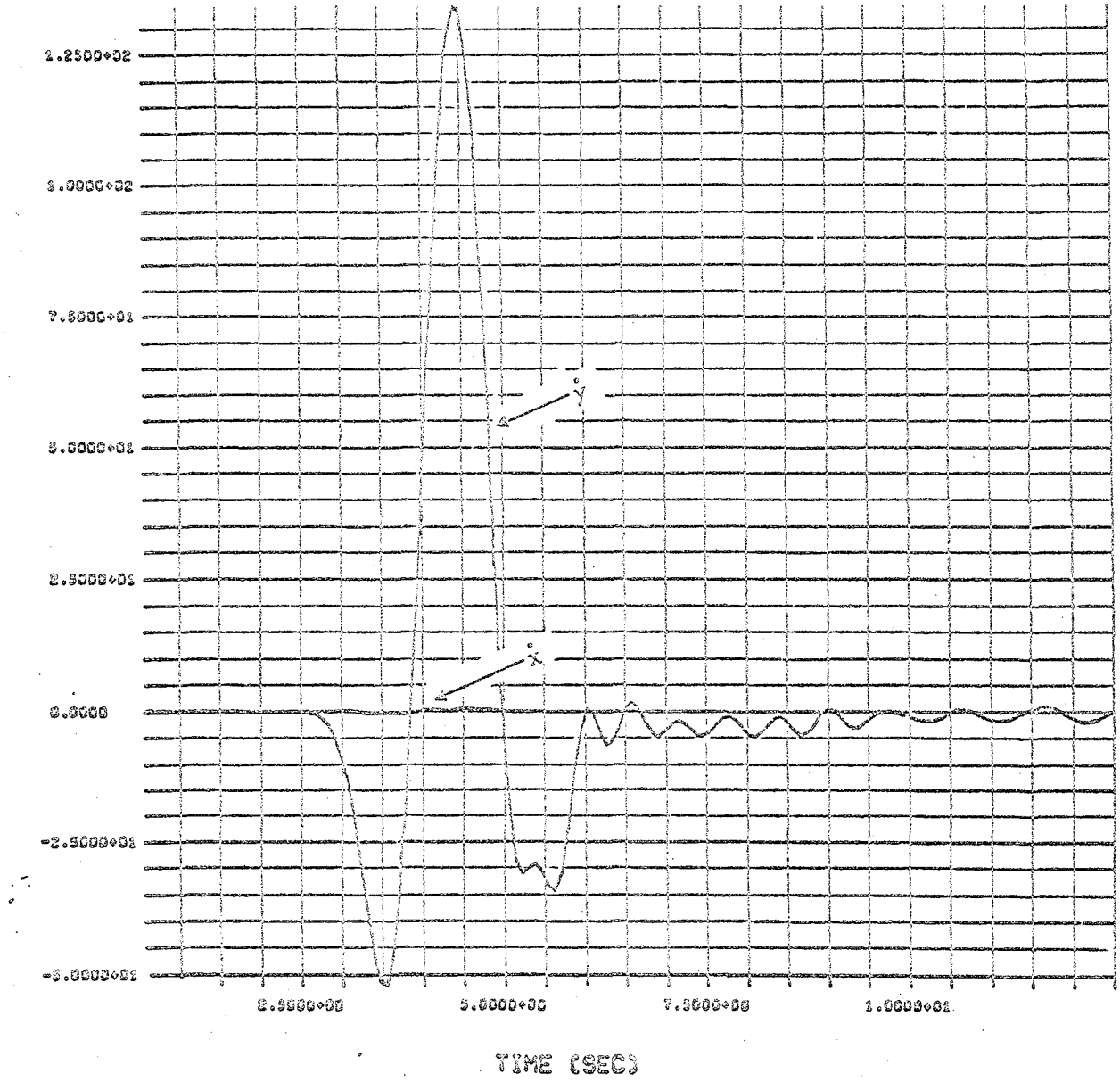

Figure 8. Particle velocity at Station 1, calculation 5B.

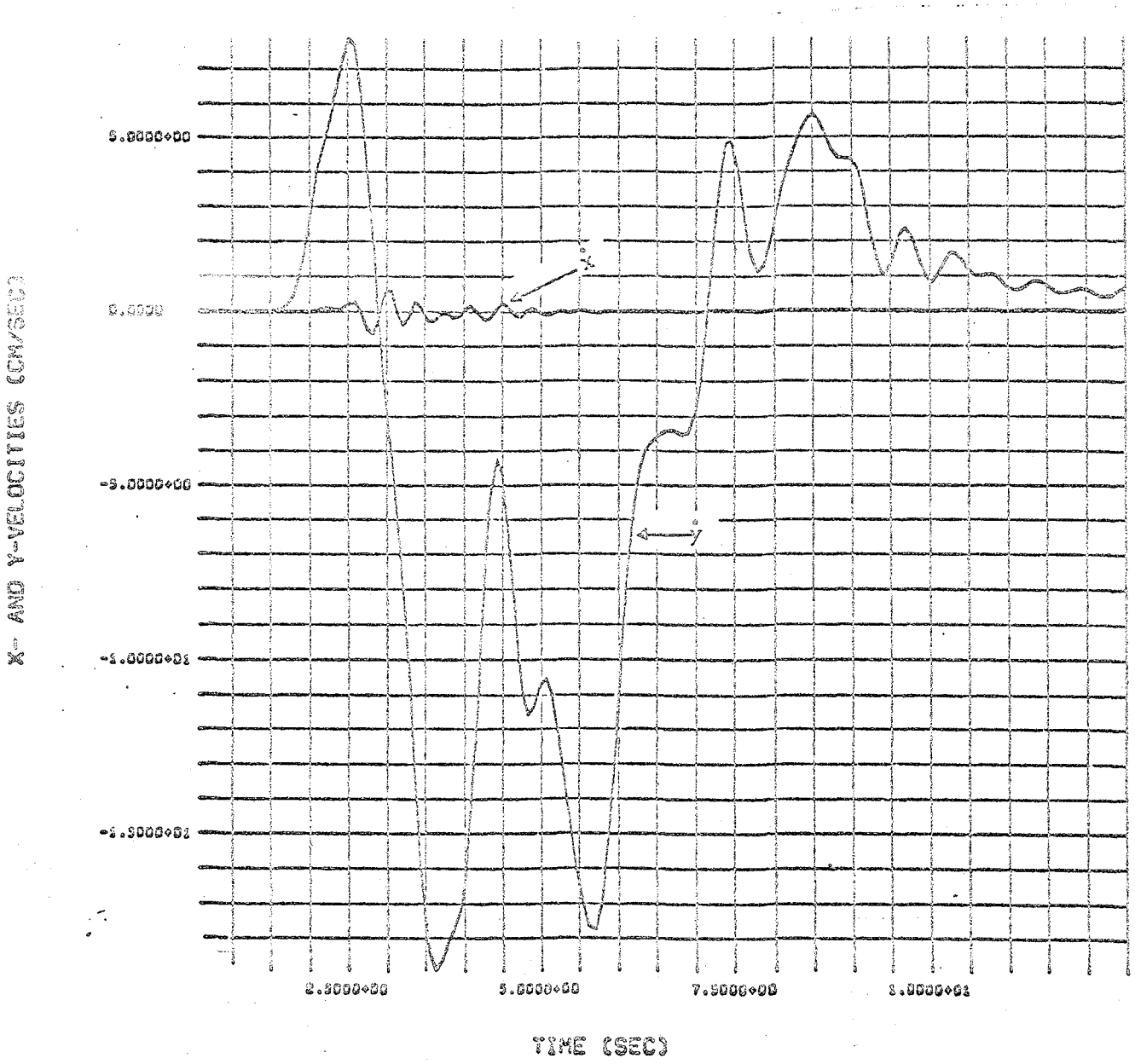

Figure 9. Particle velocity at Station 5, calculation 5B.

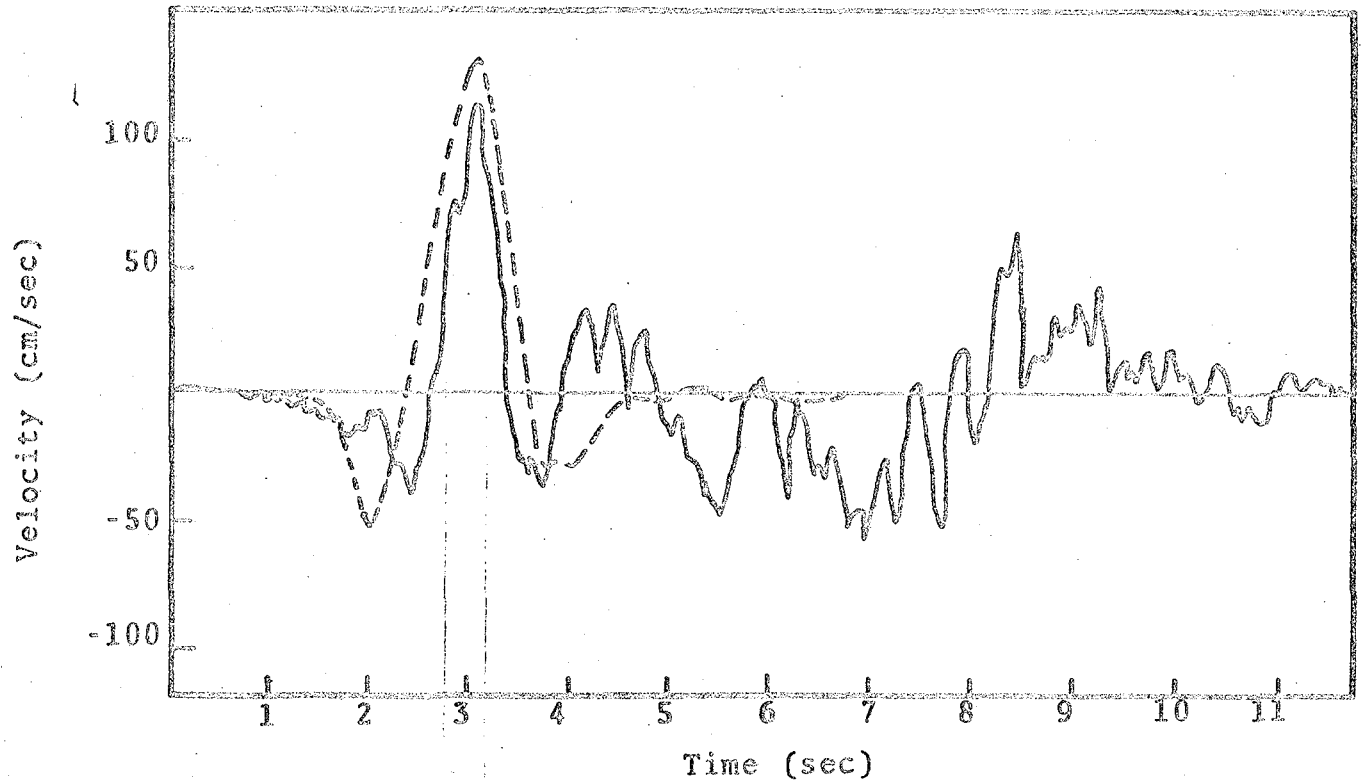

Figure 10. Comparison of free field particle velocity at Station 1, calculation 5B, with Pacoima Dam seismogram.

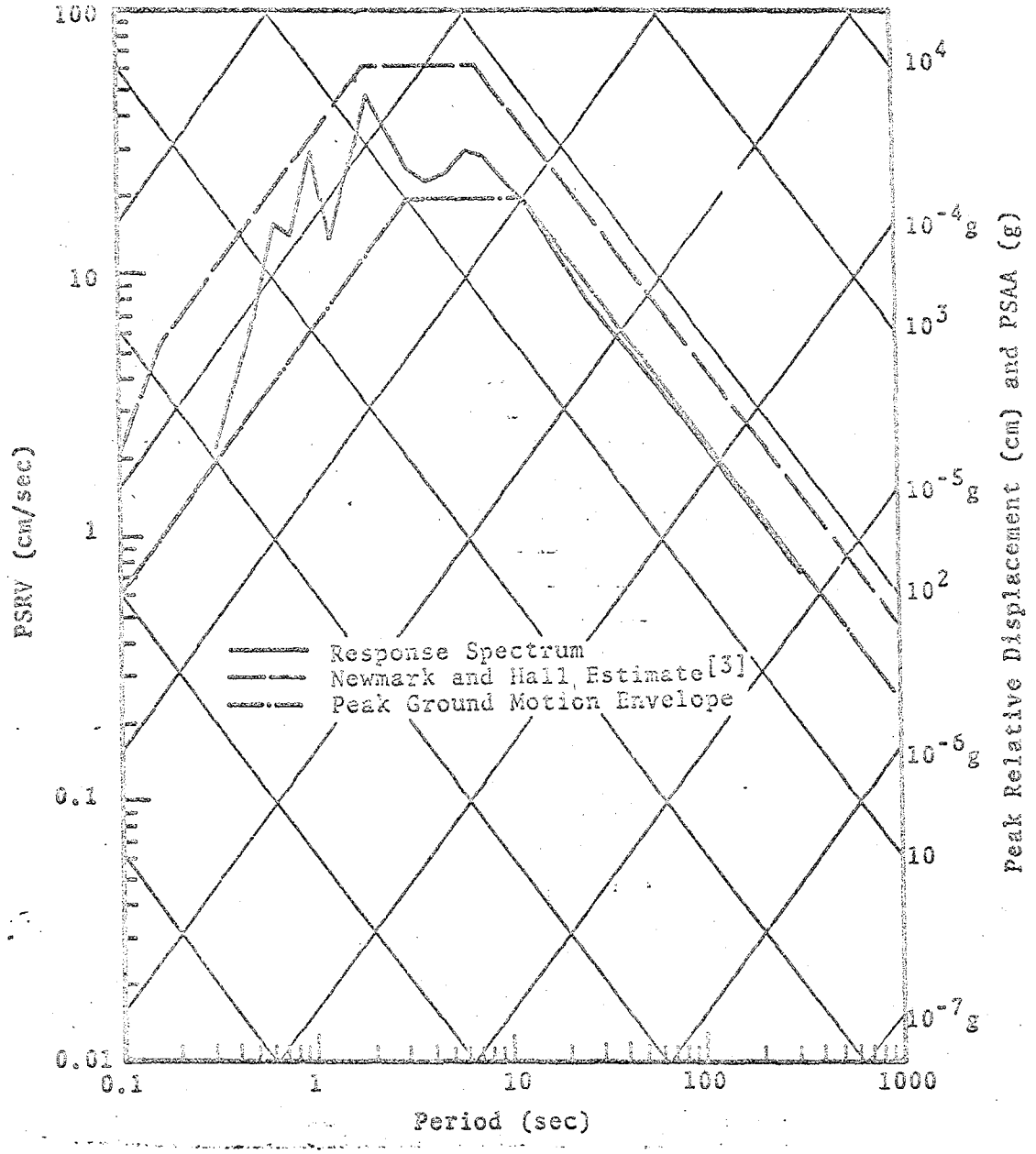

Figure 11. Response spectrum from calculation 5B, Station 5, with 1 percent critical damping.

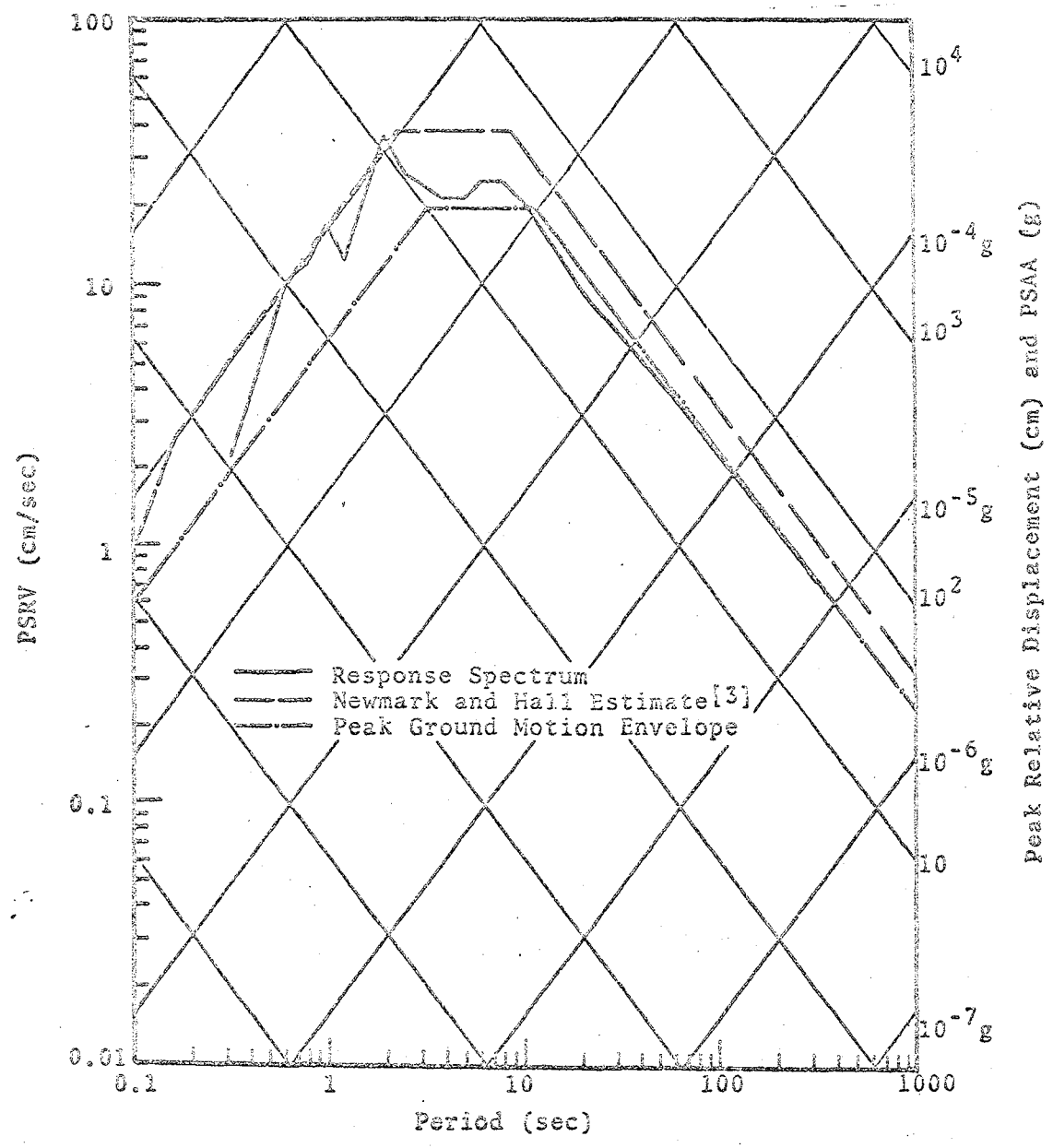

Figure 12. Response spectrum from calculation 5B, Station 5, with 5 percent critical damping.

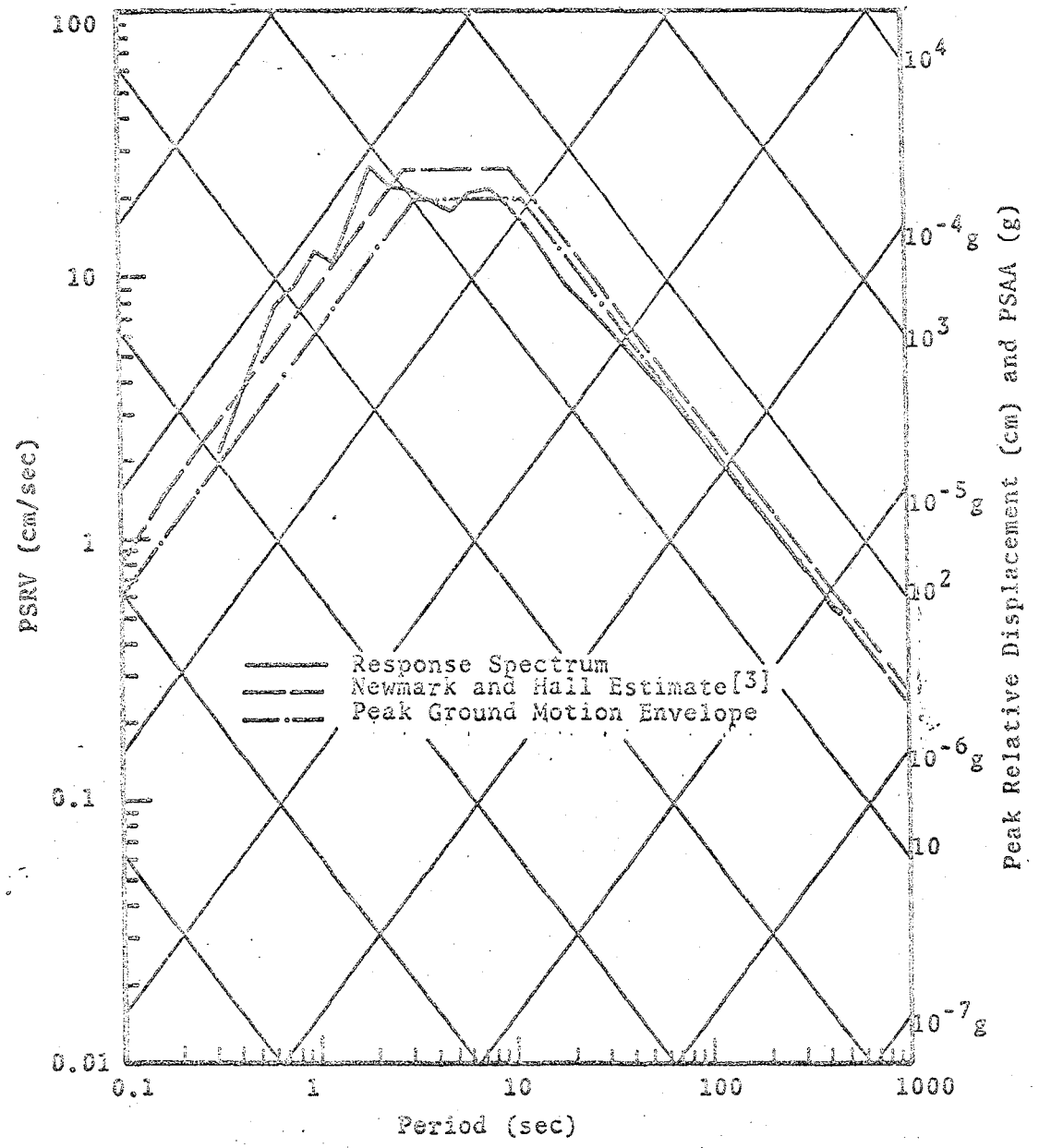

Figure 13. Response spectrum from calculation 5B, Station 5, with 10 percent critical damping.

10 percent damping. Newmark and Hall[3] have defined a procedure for generating an envelope which a response spectrum should not exceed. According to their technique an estimate is made of peak ground acceleration, velocity and displacement for a given site. These values of peak ground motion are then amplified by a factor which is a function only of the fractional damping of the oscillator.

The peak ground motion envelope at Station 5 and the resulting design spectrum of Newmark and Hall are included in Figs. 11, 12 and 13. For 1 percent and 5 percent damping the design spectrum of Newmark and Hall is a conservative estimate of the response spectrum. However, for 10 percent damping their technique under estimates the response spectrum for frequencies greater than 0.5 Hz. Similar comparisons have been made at each station for all the calculations listed in Table I. The Newmark and Hall procedure has been found acceptable for oscillator damping $\leq$ 5 percent. For 10 percent damping, failure of their technique is quite routine in the amplified acceleration regime of the design spectrum. Increasing the peak acceleration amplification factor for damping greater than 5 percent should be considered.

DEPENDENCE OF THE RESPONSE SPECTRUM ON FAULT PARAMETERS

The primary motivation for developing a deterministic earthquake model is to determine how the robust, predictable features of earthquake ground motion depend on the parameters

in the model. The parameters varied to date have been fault length (L), rupture velocity (V_R) and dynamic stress drop ($\tau_0 - \tau_K$). Scaling of peak particle velocity, the center frequency and the quality factor of the response spectrum in terms of these parameters will now be addressed.

Peak particle velocity was determined at all stations 10 km from the center of the fault. Figure 14 shows this peak ground motion plotted versus the product of rupture velocity and dynamic stress drop. The functional relation seems to be linear over at least a factor of four variation in the abscissa. As noted earlier, peak particle velocity changes by approximately an order of magnitude between Stations 1 and 5 for the same earthquake.

For each of the response spectra calculated for 10 percent damping, the peak PSRV was identified. To the left of this peak, at the lower period T_1, exists a point at which the PSRV is one half its maximum value; to the right, the longer period T_2 can be found in a similar fashion. The center period of the response spectrum was then defined by

$$T_C = \frac{1}{2}\left(T_1 + T_2\right) \tag{4}$$

By analogy to the quality factor of a filter the definition

$$Q = \frac{T_C}{\Delta T} \tag{5}$$

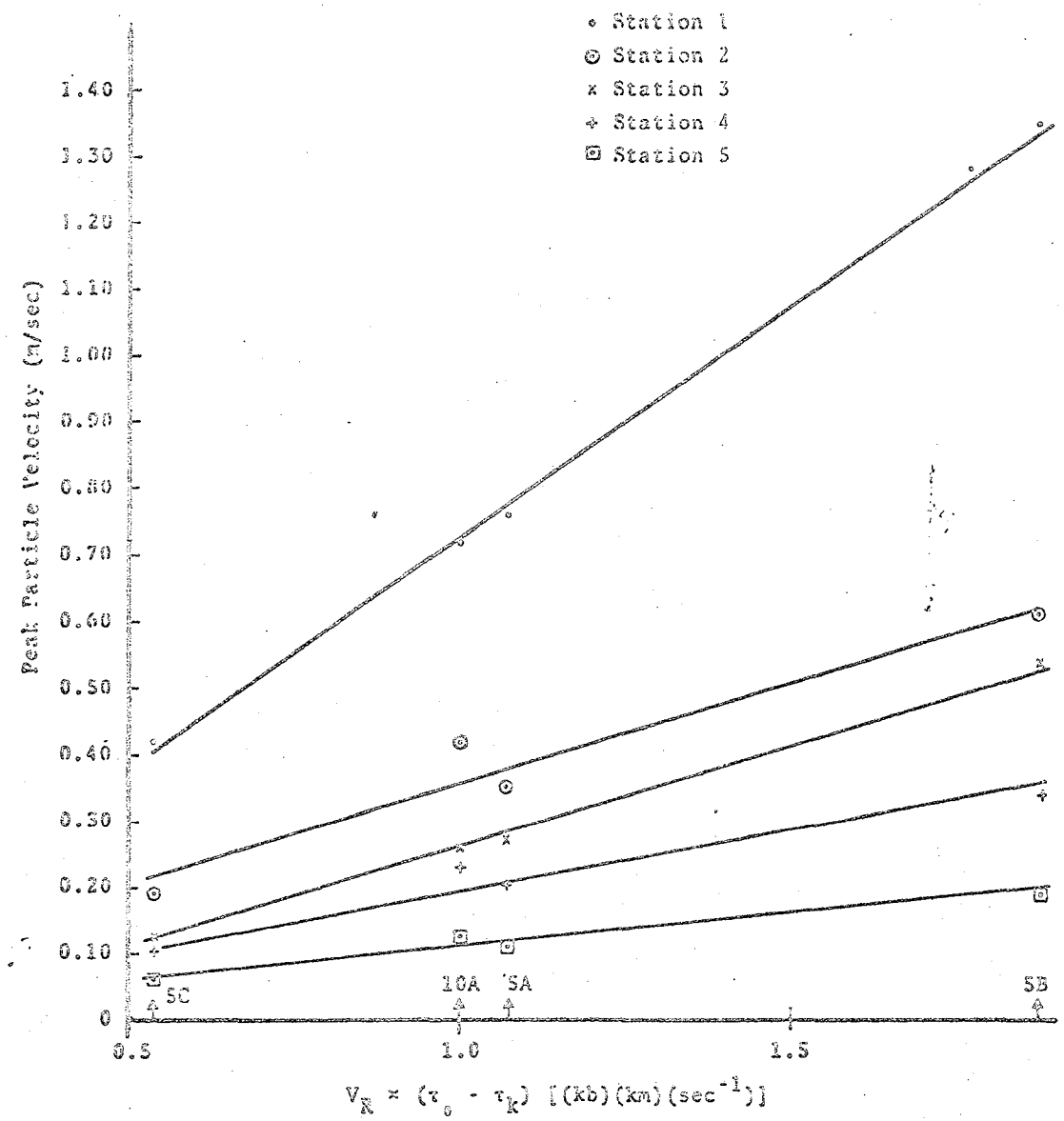

Figure 14. Peak particle velocity at a radius of 10 km from the center of the fault versus the product of rupture velocity (V_R) and dynamic stress drop ($\tau_0 - \tau_K$).

was made where

$$\Delta T = T_2 - T_1 \tag{6}$$

is the width of the excitation.

Figure 15 indicates that T_C scales linearly with L/V_R over the interval

$$1.3 \leq \frac{L}{V_R} \text{ (sec)} \leq 5 \tag{7}$$

The Doppler effect, produced by the finite rupture velocity, causes the center period of the response spectrum to strongly depend on aximuth. For the same earthquake, T_C varies by at least a factor of four between stations located at opposite ends of the fault trace.

The scaling of the quality factor, Q, of the response spectrum has been found to depend not only on fault parameters but also on the predominant wave type (P or S) responsible for the ground motion at a given azimuth. Figures 5, 6 and 7 show that ground motion at Stations 1, 3 and 5 should be predominately S. The Q of these stations scales linearly with V_R^2/L as shown in Fig. 16. Station 2 is located on a P wave lobe and the Q of this station is shown in Fig. 17 to scale inversely as the fault length.

These results suggest that

$$Q_{P,S} \sim \frac{V_R}{L} \; a_{P,S} \tag{8}$$

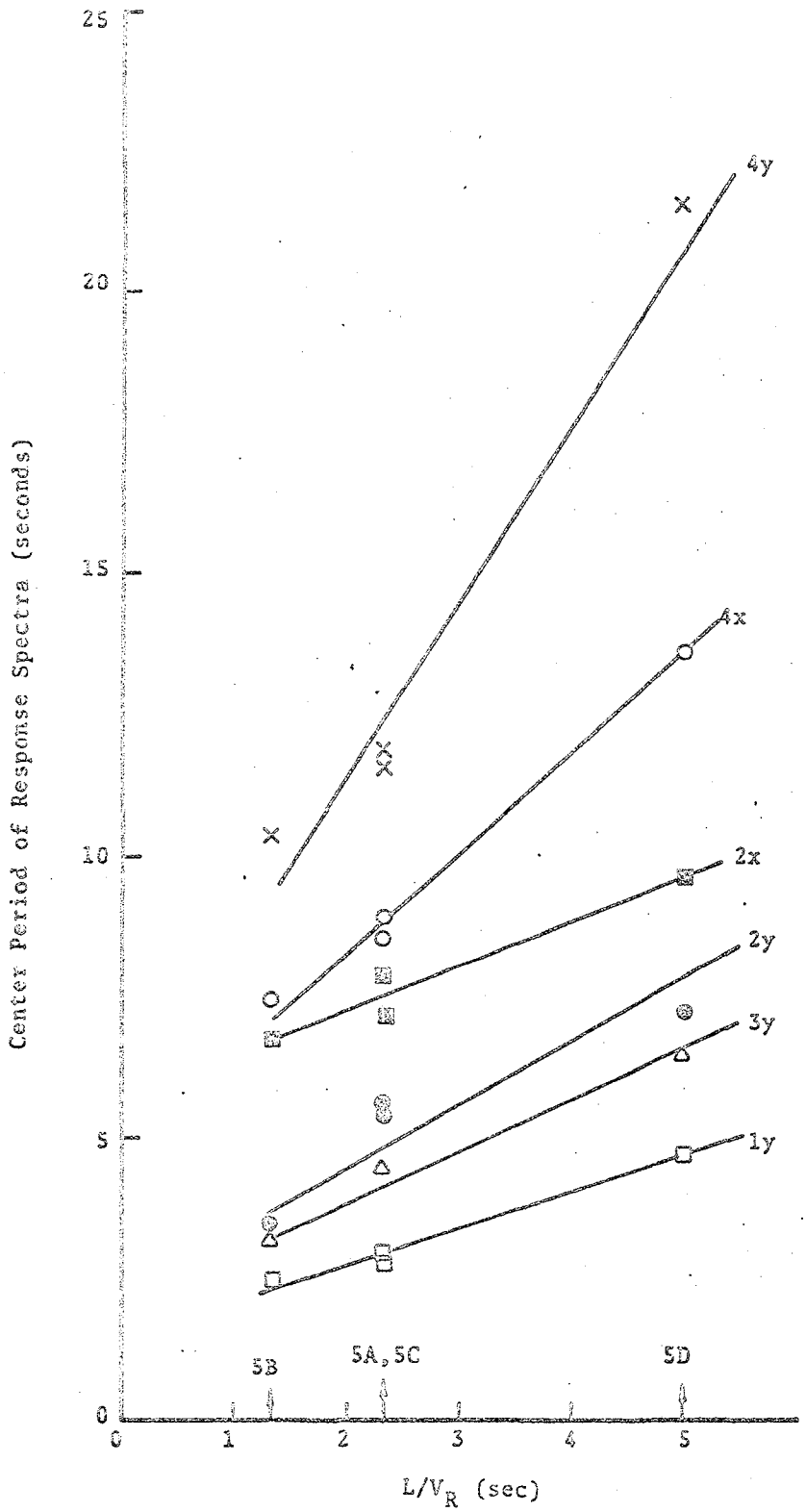

Figure 15. Center period or response spectrum versus the ratio of fault length (L) to rupture velocity (V_R).

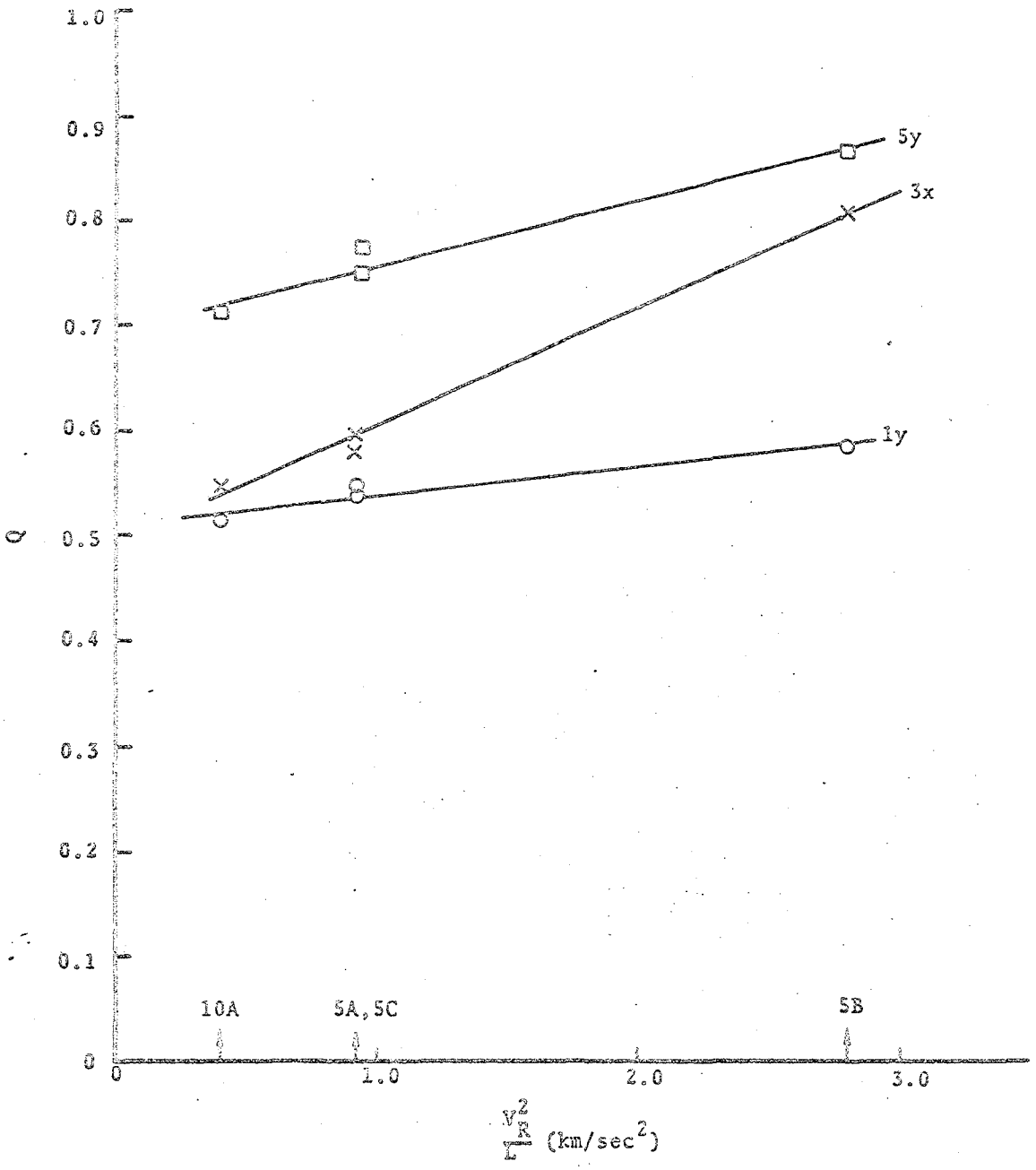

Figure 16. The quality factor of the response spectrum for stations located on an S wave lobe.

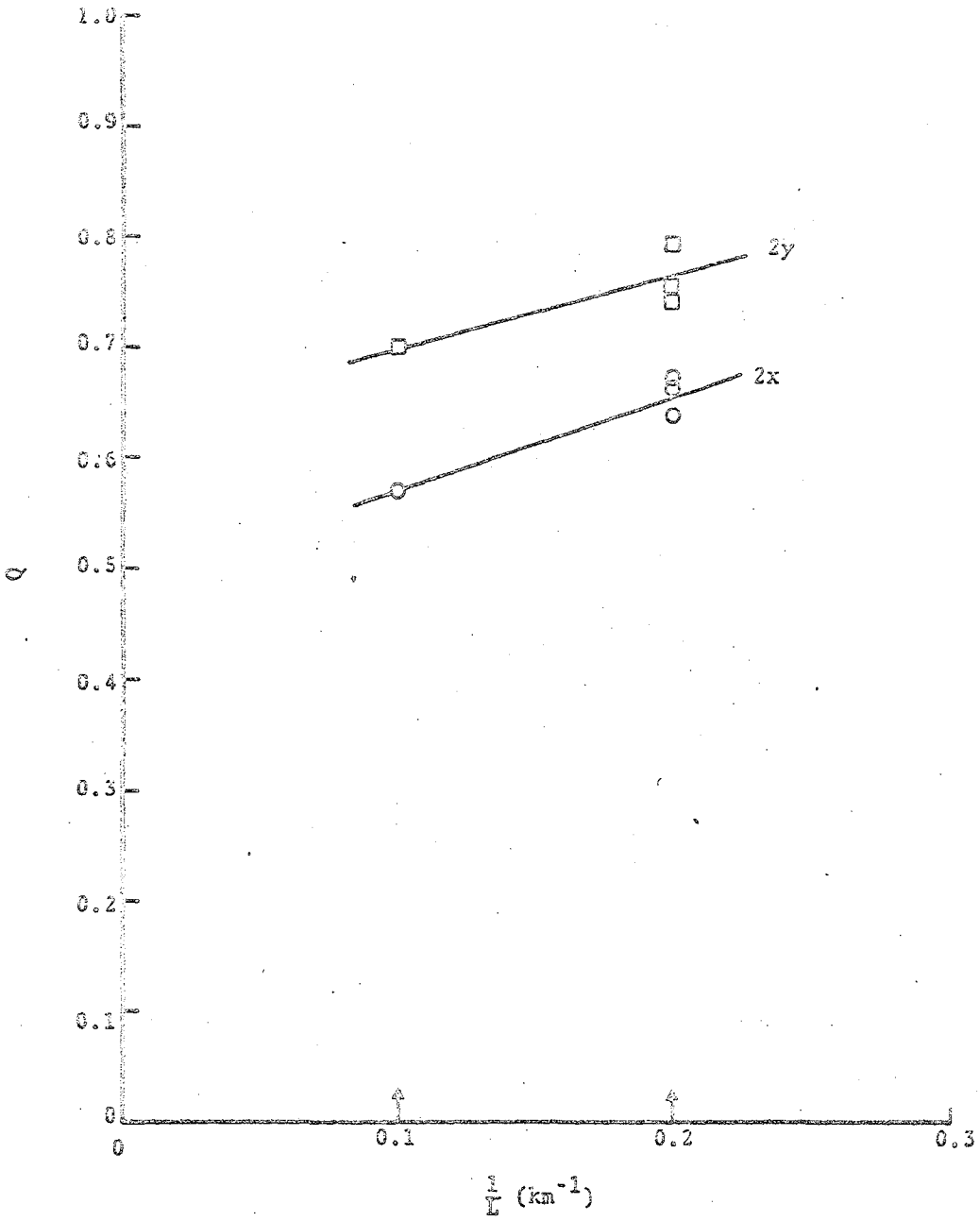

Figure 17. The quality factor of the response spectrum for stations located on a P wave lobe.

where

$$a_P = \frac{\alpha}{V_R} \tag{9}$$

$$a_S = \frac{V_R}{\beta} \tag{10}$$

Ground motion and response spectra dependence on compressional wave velocity, α, and shear wave velocity, β, has not been established from the calculations run to date. Confirmation of Eq. (8) and inclusion of near source material properties into ground motion and response spectra scaling will require an additional parameter study.

Figure 18 shows the maximum azimuthal variation in response spectra obtained from the earthquake model and compares these calculated response spectra to those obtained[26] at Glendale, California from the San Fernando earthquake. No attempt was made to match the peculiarities of the Glendale site including epicentral distance and source to site geology. Therefore, a detailed comparison with the calculated response spectra is not appropriate. However, it is interesting to note that the center periods of the observed and calculated response spectra differ by a factor of two. It is not necessary to invoke site amplification effects to explain the difference. The results shown in Fig. 15 indicate that decreasing the fault length, used in the 5B calculation, to approximately 2.5 km would be sufficient to produce a 1 Hz peak in the response spectrum.

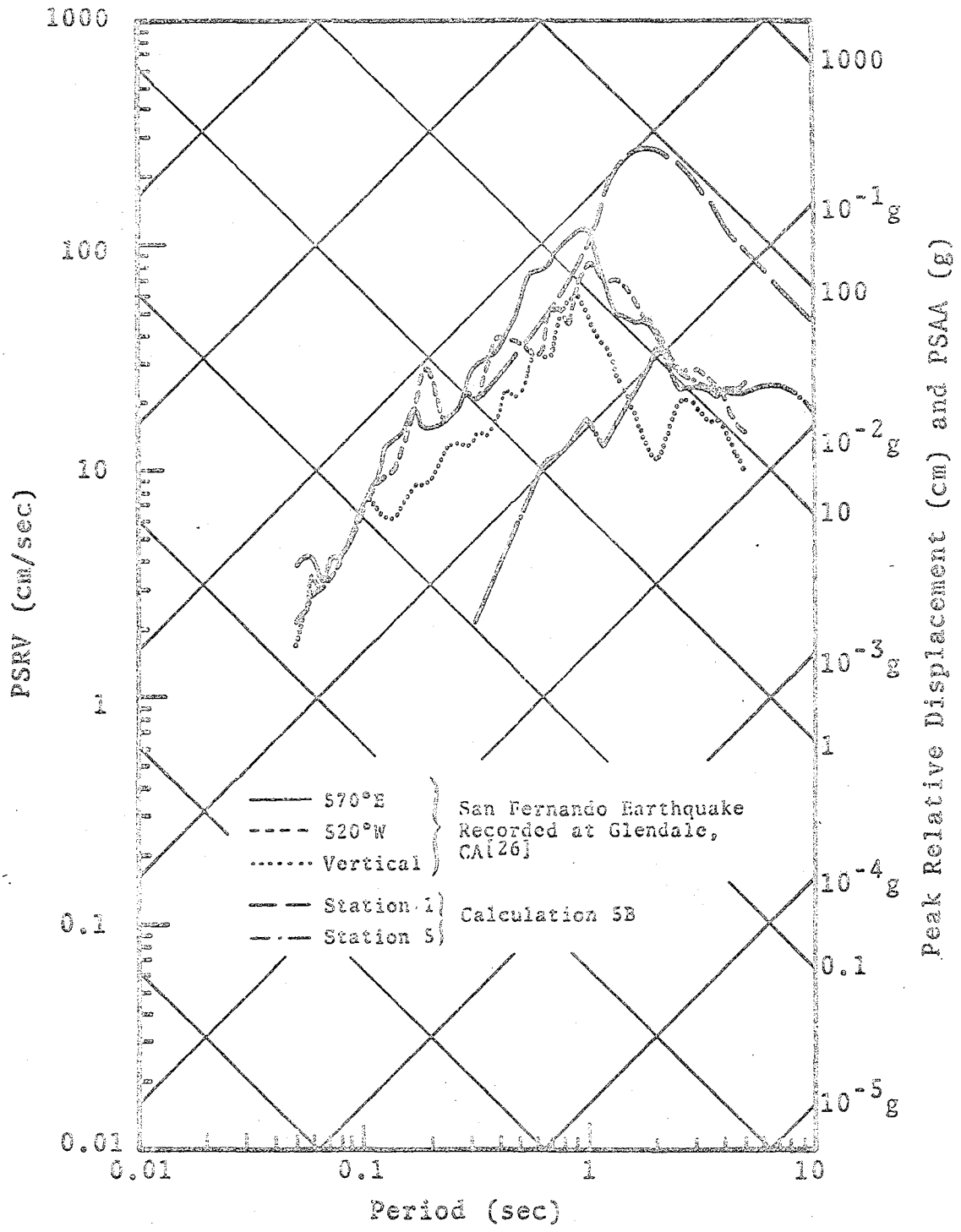

Figure 18. Response spectra at Stations 1 and 5, calculation 5B, compared to those obtained at Glendale, Calif. from the San Fernando earthquake (5 percent damping).

CONCLUSIONS

A deterministic earthquake model which merges appropriate results and techniques from computational physics and nonlinear rock mechanics offers the possibility of providing acceptable design information at sites located near the epicenter.

The computational physics aspect of the model removes the mathematics from the stress wave propagation portion of the problem. Utilization of data from rock mechanics experiments places the necessary constraints on the parameters in the model.

Future earthquake oriented research in these disciplines should be directed toward determining the fault parameters and geologic environments required to match existing design earthquakes. The constraints placed on the parameters in the model would then provide a consistent basis for obtaining design criteria at a specific site.

ACKNOWLEDGMENTS

Development of the earthquake model was supported by the Advanced Research Projects Agency of the Department of Defense and was monitored by the Air Force Office of Scientific Research under Contract No. F44620-72-C-0051. The analysis of the response spectra resulting from this model was possible due to support from the National Science Foundation Grant No. 43673. The encouragement and constructive criticism received

from participants at the ARPA/AFOSR Near Field Meetings is gratefully acknowledged. Formulation of the earthquake model resulted from highly stimulating discussions with Professor Charles B. Archambeau, Cooperative Institute for Research in Environmental Sciences (CIRES), University of Colorado, on the nature of the earthquake source.

APPENDIX I

Plastic flow is due to the inability of real materials to support unlimited values of shear stress. In the code the deviatoric stress components are modified such that the resulting stress state is consistent with a Mises yield criterion.

If the second deviatoric invariant (J) is greater than a specified value (Y/3), then

$$S_{ij} = \hat{S}_{ij} \frac{Y}{\sqrt{3J}} \left(J > \frac{Y^2}{3} \right) \tag{1}$$

where S_{ij} is the adjusted stress deviator

$\hat{S}_{ij}$ is the stress deviator calculated by assuming that the total strain rate is elastic, and

$$J = \frac{1}{2} (\hat{S}_{ij} \hat{S}_{ji}) \tag{2}$$

For a triaxial test, Y corresponds to the maximum allowable stress difference at failure.

Rupture initiation is modeled by accumulating the difference between $\sqrt{3J}$ and Y during yielding. When this accumulation reaches a specified value then the point at the fault surface enters the slip routine. Between two consecutive cycles, n and n+1, the accumulation takes the form

$$\begin{aligned} e^{n+1} &= e^n + \frac{\sqrt{3J} - Y}{Y}, \quad \left(J > \frac{Y^2}{3} \right) \\ e^{n+1} &= e^n \qquad\qquad \left(J \leq \frac{Y^2}{3} \right) \end{aligned} \tag{3}$$

Rupture occurs if

$$e^{n+1} \geq W \tag{4}$$

where W is a specified function of distance from the initial point of rupture.

Equation (3) is similar to a plastic work criterion, where the plastic work (E^{n+1}) is given by

$$E^{n+1} = E^n + \frac{Y^2}{3\mu} \frac{\sqrt{3J} - Y}{Y} \tag{5}$$

Equations (3) and (5) differ only by the factor $Y^2/3\mu$.

We have been successful in both controlling rupture velocity and reducing the stress concentrations at the end of the fault by allowing W, in Eq. (4), to be a specified function of distance from the point of rupture initiation. The functional form that has been used is

$$W = 6c \left(\frac{x + L/2}{d}\right) \left[\frac{1}{2} - \frac{1}{3} \frac{x + L/2}{d}\right] \quad 0 \leq x + \frac{L}{2} \leq \frac{d}{2} \tag{6a}$$

$$= \frac{c}{2} \left[-\frac{1}{2} + 3 \frac{x + L/2}{d}\right] \quad x + \frac{L}{2} \geq \frac{d}{2}$$

where L, c and d are input parameters. The rupture is constrained to lie between $-L/2 \leq x \leq L/2$, where L is the fault length.

REFERENCES

1. Jennings, P. G., G. W. Housner and N. C. Tsai, "Simulated Earthquake Motions for Design Purposes," Proceedings 4th World Conference on Earthquake Engineering, Santiago, Chili, A-1, pp. 145-160 (1969).
2. Ruiz, P. and J. Penzien, "Stochastic Seismic Response of Structures," J. of Engng. Mech. Div., ASCE 97, pp. 441-456 (1971).
3. Newmark, N. M. and W. J. Hall, Procedures and Criteria for Earthquake Resistant Design," Proceedings Building Practices for Disaster Mitigation, Boulder, Colorado, pp. 209-236 (1972).
4. Hofmann, R. B., "State-of-the-Art for Assessing Earthquake Hazards in the United States," Report 3, Factors in the Specification of Ground Motions for Design Earthquakes in California, Paper S-73-1, U. S. Army Engineer Waterways Experiment Station (1974).
5. Saragoni, G. R. and G. C. Hart, "Simulation of Artificial Earthquakes," Int. J. Earthquake Engineering Struct. Dyn. 2, pp. 249-267 (1974).
6. Maenchen, G. and S. Sack, "The TENSOR Code," Methods in Computational Physics 3, Academic Press, New York, pp. 181-210 (1964).
7. Wilkins, M. L., "Calculation of Elastic Plastic Flow," Methods in Computational Physics 3, Academic Press, New York, pp. 211-263 (1964).

8. Cherry, J. T., S. Sack, G. Maenchen and V. Kransky, "Two Dimensional Stress-Induced Adiabatic Flow," Lawrence Radiation Laboratory Report UCRL-50987, Livermore, California (1970).

9. Andrews, D. J., "A Numerical Study of Tectonic Stress Release by Underground Explosions," Bull. Seism. Soc. Am. 63, pp. 1375-1391 (1973).

10. Cherry, J. T. and W. R. Hurdlow, "Numerical Simulation of Seismic Disturbances," Geophysics 31 (1966).

11. Boore, D. M., "Finite Difference Methods for Seismic Wave Propagation in Heterogeneous Materials," Methods in Computational Physics, Academic Press, New York, pp. 1-37 (1972).

12. Cameron, I. G. and G. C. Scorgie, "Dynamics of Intense Underground Explosions," J. Inst. Math. Appls. 4, pp. 194-222 (1968).

13. Cherry, J. T. and F. L. Petersen, "Numerical Simulation of Stress Wave Propagation from Underground Nuclear Explosions," Symposium on Engineering with Nuclear Explosives CONF-700101, 1, pp. 142-220 (1970).

14. Sandler, I. and F. L. DiMaggio, "Material Models for Rocks," Defense Nuclear Agency Report DASA-2595 (1970).

15. Riney, T. D., G. A. Frazier, S. K. Garg, A. J. Good, R. G. Herrmann, L. W. Morland, J. W. Pritchett, M. H. Rice, and J. Sweet, "Constitutive Models and Computer Techniques for Ground Motion Predictions, Defense Nuclear Agency Report DNA-3180F (1973).

16. Butkovich, T. R., "Calculation of the Shock Wave from an Underground Nuclear Explosion," J. Geophys. Res. 70, pp. 885-891 (1965).

17. Cherry, J. T., "Computer Calculations of Explosion-Produced Craters," Int. J. Rock Mech. Min. Sci. 4, pp. 1-22 (1967).

18. Crowley, B. K., "Effects of Porosity and Saturation on Shock Wave Response in Tuff," Int. J. Rock Mech. Min. Sci. 10, pp. 437-467 (1973).

19. Cherry, J. T., T. C. Bache, C. B. Archambeau and D. G. Harkrider, "A Deterministic Approach to the Prediction of Teleseismic Ground Motion from Nuclear Explosions, Defense Nuclear Agency Report DNA-3321F (1974).

20. Schnabel, P., H. B. Seed and J. Lysmer, "Modification of Seismograph Records for Effects of Local Soil Conditions," Bull. Seism. Soc. Am. 62, pp. 1649-1664 (1972).

21. Benioff, H., "Earthquake Source Mechanisms," Science 143, pp. 1399-1406 (1964).

22. Heard, H. C., "The Influence of Environment on the Inelastic Behavior of Rocks," Symposium on Engineering with Nuclear Explosives CONF-700101, 1, pp. 127-141 (1970).

23. Johnson, T., F. T. Wu and C. H. Scholz, "Source Parameters for Stick Slip Earthquakes," Science 179, (1973).

24. Byerlee, J. D., "Static and Kinetic Friction of Granite at High Normal Stress," Int. J. Rock Mech. Min. Sci. 7, pp. 577-582 (1970).

25. Hanks, T. C., "The Faulting Mechanism of the San Fernando Earthquake," J. Geophys. Res. 79, pp. 1215-1229 (1974).

26. Scholl, R. E., "Statistical Analysis of Low-Rise Building Damage Caused by the San Fernando Earthquake," Bull. Seism. Soc. Am. 64, pp. 1-23 (1974).